

# AN ANALYSIS OF THE PERFORMANCE OF DIFFERENT DPSK MODULATION DATA FORMATS USING CROSS-POLARIZATION MODULATION BASED 80 Gb/s ALL-OPTICAL WAVELENGTH CONVERSION IN A SINGLE WIDEBAND SOA

SAROJINI R<sup>1\*</sup>, SIVANANTHA Raja A<sup>2</sup> and SELVENDRAN S<sup>3</sup>

<sup>1</sup>Government College of Engineering Srirangam, Trichy, Tamilnadu, India

<sup>2</sup>Alagappa Chettiar Government College of Engineering and Technology, Karaikudi, Tamilnadu, India.

<sup>3</sup>Vellore Institute of Technology, Chennai, Tamilnadu, India.

\*Corresponding author: [sarojiniraju18@gmail.com](mailto:sarojiniraju18@gmail.com)

**Abstract:** At key optical network nodes the efficient deployment of WDM/DWDM technologies can be made possible by wavelength conversion. In this research, Cross-Polarization Modulation (XpolM) based All-Optical Wavelength Conversion (AOWC) using wide band Semiconductor Optical Amplifier (SOA) is obtained. The effectiveness of various optical differential phase modulations on wavelength conversion is analysed. NRZ-DPSK/DPSK, 33%RZ-DPSK, 50%RZ-DPSK and 67%RZ-DPSK/CSRZ-DPSK are investigated here. The data rate is 80 Gb/s and the conversion bandwidth is 1.04 nm. The analysis is extended for Linear, Lorentzian and No-approximation material gain simulation models. The NRZ-DPSK performs better in terms of maximum coupled intensity and ellipticity. CSRZ-displays a power spectral gain of up to 12 dB and shows narrower spectral width.

**Key words:** Semiconductor Optical Amplifier (SOA), Cross-Polarization Modulation (XpolM), All-Optical Wavelength Conversion (AOWC), Differential Phase Shift Keying (DPSK), Carrier Suppressed Return-to-Zero DPSK (CSRZ-DPSK).

## 1 INTRODUCTION

Optical communication technology has dominated the communication sector in the past few decades. Multiplexing concepts like WDM (Wavelength Division Multiplexing), DWDM (Dense Wavelength Division Multiplexing) and SM (Spatial Modulation) are employed to effectively utilize fiber bandwidth. The wavelength converters have emerged as the fundamental functionality of wavelength-routed networks to make the network transparent and allow interoperability. Wavelength converters resolve the issue of data contention [1], [2]. Optical cross-connects (OXC), which are essential parts of wavelength-division multiplexing (WDM) networks, frequently incorporate wavelength converters. OXCs efficiently route traffic and address contention problems in large-scale optical networks by using wavelength converters to change incoming signals from one input port to one or more output ports. In this research optical nonlinearity is used with optical gating approach to realize the wavelength conversion functionality. The saturated Semiconductor Optical Amplifier (SOA) is used as an optical gate [3]. The optical nonlinearities refer to the ability of a device to alter its characteristics in response to the optical signal intensity. These modifications can be applied to another optical signal at different wavelength called probe signal. After wavelength conversion the information is obtained in the output probe signal. This approach offers transparency and acceptably works well

over the bandwidth of 100 nm, which is the amplifier gain bandwidth. Cross-Gain Modulation (XGM) [4], [5], Cross-Phase Modulation (XPM) [4], and Cross-Polarization Modulation (XpolM) are the SOA nonlinearities which can be realized in the optical gating approach [6], [7].

The SOA exhibits very fast carrier dynamics, which happen in pico second time scale. Hence the wavelength conversion at the rate of Gb/s is possible [8]. The main advantage of this optical gating is that it is abstractly simple. In this research, XpolM has been considered as a necessary nonlinearity for wavelength conversion in the optical gating approach.

Finding the most appropriate and data modulation format is crucial when high speed wavelength converters are taken into consideration. Here, DPSK is considered as it has a good dispersion tolerance and only needs half the typical optical power in optical networks [9]. It also offers improved receiver sensitivity and transmission performance. If a balanced receiver is employed for the detection, a nearly 3 dB lower OSNR is sufficient to attain the specified BER [10]. This is the most apparent advantage of DPSK over OOK. [11], [12] demonstrated that for an optically preamplified receiver, at a BER of  $10^{-9}$ , the quantum limit is 41 photons/bit for OOK without filtering. This quantum limit reduces to 22 photons/bit for DPSK with balanced detection.

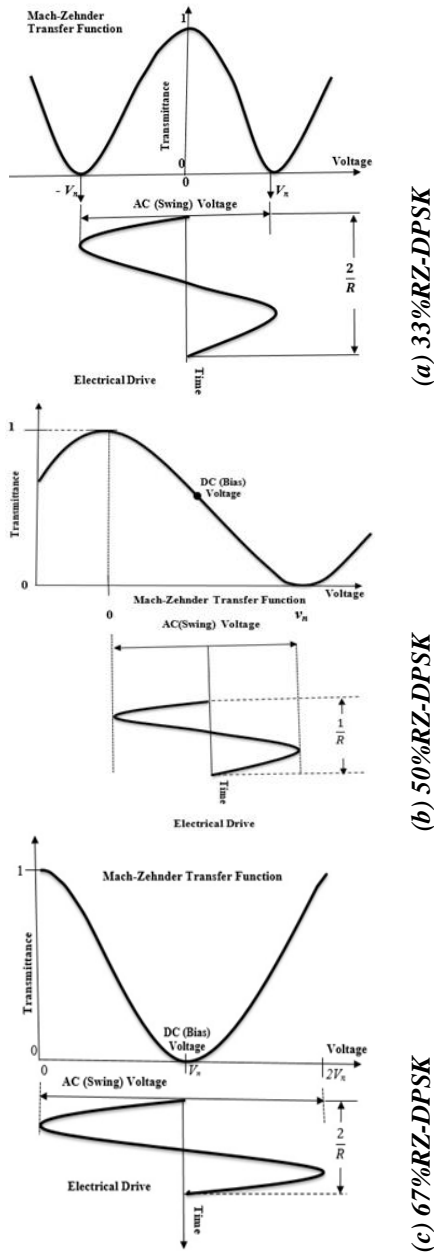


Figure 1 Drive setting functions for RZ-DPSK signals

Hence for the optical high data rate systems that employ WDM / DWDM techniques, DPSK provides many advantages over conventional OOK format with the added design complexity in the transmitter and receiver. The relative merits of various DPSK formats and the system impairments were studied [13], [14]. The differential phase modulation formats like NRZ-DPSK/DPSK, 33%RZ-DPSK, 50%RZ-DPSK and 67%RZ-DPSK/CSRZ-DPSK are considered here. This investigation is distinctive as it evaluates the performance of different DPSK data modulations in the context of XpolM-based wavelength conversion.

This study is also broadened to take different material gain approximation models into account; Linear, Lorentzian, and no-approximation models. The wavelength conversion is accomplished at an 80 Gb/s data rate. 1.04 nm is the

conversion bandwidth. The inference of this research paper is that CSRZ-DPSK is the viable option because it results in significantly higher power spectral gain up to 12 dB. More specifically, in the No-approximation material gain simulation model, this CSRZ-DPSK data wavelength conversion exhibits a smaller spectral main lobe width.

## II OPTICAL RZ-DPSK GENERATION

Optical RZ modulation has three general forms based on its duty cycle. They are 33% RZ (RZ with 33% duty cycle), 50% RZ (RZ with 50% duty cycle), and 67%RZ (RZ with 67% duty cycle), which is popularly known as carrier-suppressed RZ (CSRZ) [15]. The driving functions for different RZ-DPSK with the MZM (Mach-Zehnder Modulator) transfer function is shown in Figure 1. It is shown that the drive signal is biased at various specific transmission points of MZM based on its duty cycle. These functions ensure the constructive and destructive interferences for the bit 1 and 0.

The drive signal or pulse carving function is defined by equation (1)

$$V_o(t) = A \cos(2\pi v_c t - \theta) \tag{1}$$

where  $A$  is the amplitude which is set at 1 V;  $v_c$  is the frequency of the RZ drive signal voltage;  $\theta$  is the phase offset as a fraction of  $V_\pi$ . The appropriate frequency and phase of the driving functions are given in Table 1. Figure 1 (a) shows that the 33%RZ signal is biased at the 100% transmission point of the MZM transfer function. The swing voltage is twice as compared to the 50% RZ bias function. Hence the frequency  $v_c$  is set at  $B(\text{bit rate})/2$ , and the phase is at  $-90^\circ$ . During each transition between the nodes of the MZM transfer function, one modulated pulse is generated. As shown in Figure 1 (b), the 50% RZ signal is biased at the half-maximum transmission point of the MZM transfer function. Hence the frequency  $v_c$  is set at  $B$  bit rate, and the phase is at  $-90^\circ$ . Figure 1 (c) shows that the 67% RZ signal is biased at the 100% transmittance point of the MZM transfer function, as in the case of the 33% RZ signal. But 67%RZ drive is biased at the null transmittance point of the MZM transfer function. Hence the frequency  $v_c$  is set at  $B$  bit rate  $/2$ , and the phase is at  $0^\circ$ .

Table 1 Parameters used

Parameter	Duty Cycle		
	33%	50%	67%
Frequency $v_c$	40 GHz (Bit rate)	80 GHz (Bit rate)	40 GHz (Bit rate /2)
phase $\theta$	$-90^\circ$	$-90^\circ$	$0^\circ$

The SOA is biased at the injection current of 0.37 A. In the saturation regime, carriers diffused unevenly along the active region of SOA due to the asymmetric structure. When there is a pump signal present, this distribution becomes much more distorted. The axis of the active region of the SOA determines this distribution. This distribution is further controlled by

## III EXPERIMENTAL SYSTEM ARRANGEMENT

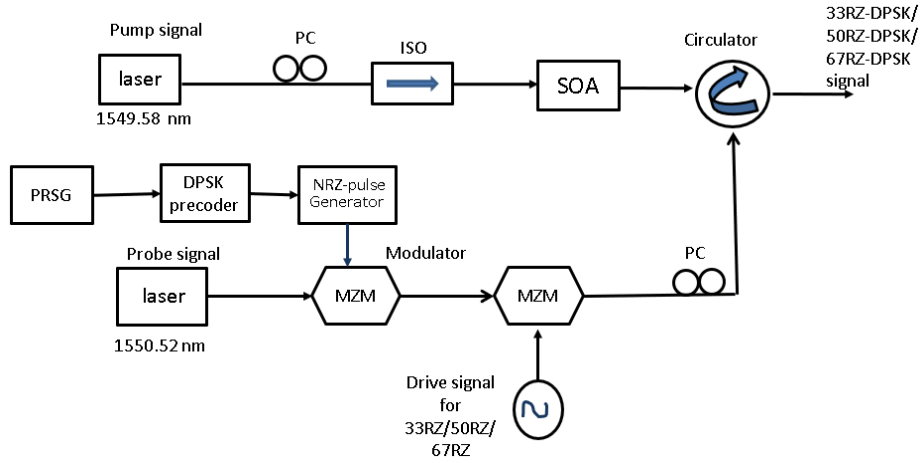


Figure 2. XpolM-based AOWC of various DPSK data modulation formats

The experimental setup of XpolM-based AOWC is shown in Figure 2. It consists of two sections; Data modulation section and wavelength converter section. The data modulation section includes an optical laser source that emits a probe signal at 1550.52 nm wavelength with 1 dBm power, a DPSK precoder and two cascaded MZM modulators. The  $2^{31}-1$  PRBS generates an 80 Gb/s bit stream which is given to the DPSK precoder.

The NRZ-DPSK data is then intensity-modulated by the combined blocks of the NRZ pulse generator and MZM. This first MZM is driven by the input probe laser of 1550.52 nm wavelength. In the generation of RZ-DPSK, the second MZM involves and performs the function of pulse carving. This pulse carving is accomplished by the RF sinusoidal signal with the appropriate frequency and the phase. In the generation of NRZ-DPSK / DPSK, the second MZM is eliminated and no driving function is used for carving. The wavelength converter section consists of the optical laser source called pump laser that emits light at 1549.48 nm wavelength, SOA and the circulator. The pump signal power is fixed with -4 dBm. The pump and the probe signals are counter-propagating into an SOA. The polarisation controller (PC) can be used to maintain the input probe signal's linear polarisation at a wavelength of 1550.52 nm. ISO (Optical Isolator) stops the back propagation of the pump signal and causes the polarization rotation. As a result, the wavelength converted signal is obtained at 1549.48 nm [16]. The parameters involved in these simulations are listed in Table 2. Different phase and gain compression are introduced on the TE and TM components when two signals, the pump and probe, are injected into the SOA at the same time. Due to Equation (2), the device gain being polarization-dependent.

$$G = (\Gamma g_m - \alpha)L \quad (2)$$

where  $\Gamma$  is the confinement factor,  $g_m$  is the material gain,  $\alpha$  represents the optical losses, and  $L$  is the device length [17]. As a result, the signal's polarisation state is altered, leading to a polarisation rotation known as Non-Linear Polarisation Rotation (NPR) [18], [19] & [20].

Table 2 Parameters used

Parameters	Value
Confinement factor	0.45
Bias current	0.37 A
Active region length	0.0006 m
Active region width	1.5 e-06 m
Active region height	0.5 e-06 m
Pump power	-4 dBm
Probe power	1 dBm

OptiSystem16 software is used for the design. The numerical simulation is done in two steps. In the first step the active region of the SOA is divided into several portions. The steady state condition is consideration at the boundaries [21]. The carrier density rate will only be controlled by the current bias level and the input flux in each SOA segment during the second step. This simulation is repeated for different material gain simulation models; Linear, Lorentzian and no-approximation of material gain. Each model has a specific carrier density profile. The parameters used in these simulation models are listed in Table 3. If the assumption made in the SOA electric field wave equation is such that there is a linear dependence between the carrier-induced susceptibility and the carrier density, then it is called linear approximation. Then the material gain coefficient  $g_m$  is related to carrier density  $N(t)$  as in the Equation (3)

$$g_m(t) = A_g [N(t) - N_0] \quad (3)$$

where  $N_0$  is the carrier density at the transparency point, and  $A_g$  is the differential gain coefficient. The net gain coefficient  $g$  is related to the material gain  $g_m$  by the Equation (4)

$$g(t) = \Gamma g_m(t) - \alpha \quad (4)$$

where  $\alpha$  is an effective loss coefficient which includes scattering and absorption losses, and  $\Gamma$  is the optical confinement factor defined as a fraction of the mode power within the active layer.

Table 3 Different material gain ( $g_m$ ) simulation model parameters of SOA

model parameters	Linear	Lorentzian.	No-approx.	unit
Gain constant $a_0$	27.8e-21	27.8e-21	-	$m^2$
Carrier density at transparency $n$	1.4e+24	1.4e+24	-	$m^3$
Gain peak wavelength $\lambda$	-	1549.52	-	nm
Gain bandwidth $\Delta\lambda$	-	122.5	-	nm
$n_1$ Active refractive index	-	-	3.2	-

In Lorentzian approximation, the material gain  $g_m$  profile follows Lorentzian line shape [21]. The Equation (5) describes the  $g_m$  in Lorentzian approximation.

$$g_m(\nu, n) = \frac{a_0(n-n_1)}{1 + \frac{(\lambda-\lambda_n)^2}{\Delta\lambda^2}} \quad (5)$$

where  $a_0$  is the gain constant,  $n$  is the carrier density,  $n_1$  is the carrier density at transparency,  $\lambda_n$  is the spectral shift,  $\Delta\lambda$  is the 3-dB bandwidth of the linear gain coefficient. The gain constant, carrier density and the gain bandwidth are not approximated in the no-approximation material gain simulation model [22].

#### IV RESULTS

The numerical simulation of AOWC using XPoIM is carried out for four different DPSK data modulation formats. NPR inside the SOA is the basic principle of the XPoIM-based wavelength conversion. This polarisation rotation may introduce additional birefringence effect inside the device cavity or waveguide asymmetry in the waveguide structure. The confinement factor is different for TE and TM modes because the active region of SOA does not have equal sides.

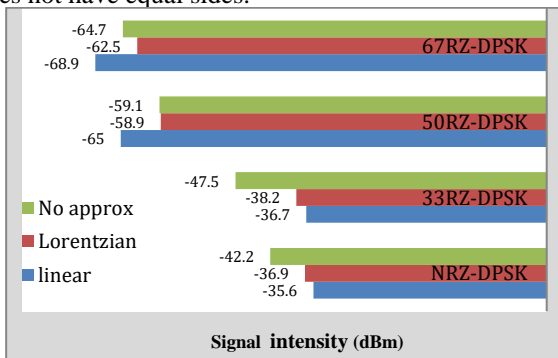


Figure 3. Signal intensity coupled into wavelength converted signal for different data formats and material gain simulation models

As the material gain directly influences the device gain which is polarization-dependent, the experiment is

extended for linear, Lorentzian approximation and No-approximation simulation models. Figure 3 shows the amount of signal intensities coupled with the wavelength converted signal for all four DPSK formats. Compared to other data formats, it is obvious that NRZ-DPSK has the highest level of intensity coupled with the converted beam. NRZ-DPSK couples at around -40 dBm, while RZ-DPSK data formats couple less. As a result, NRZ-DPSK performs better in terms of maximum intensity coupled with the converted signal.

Figure 4 shows the ellipticity profile, NRZ-DPSK shows evidence of maximum amount of polarization rotation compared. The ellipticity angle is  $\sim 31^\circ$  for NRZ-DPSK while other formats have upto  $\sim 28^\circ$ .

Figures from 5 (a) to (d) illustrate the dual power spectrum of NRZ-DPSK, 33% RZ-DPSK, 50%RZ-DPSK, and CSRZ-DPSK, respectively, for the linear material gain approximation simulation model. Similarly, Figures from 6 (a) to (d) and Figures from 7 (a) to (d) illustrate the dual power spectrums for Linear, Lorentzian and no-approximation simulation models, respectively. These figures are the visual substantiation of their power spectral gains which are numerically validated in table 4. The blue and red shifted components in these figures are attributed to the residual effects of nonlinear effect such as self-phase modulation (SPM). Other non-linear effects like cross-phase modulation (XPM) will also occur depending on their intensity level as a result of the interaction of two optical fields inside the active region of a SOA. This creates a phase noise that leads to the red and blue shifts.

Table 4 Output power spectral gain

Data format	Power gain (dB)		
	Linear	Lorentzian	No-approx
NRZ-DPSK/DPSK	-30	-31	-42
33% RZ-DPSK	-30	-27	-44
50% RZ-DPSK	-25	-20	-27
67%RZ-DPSK/(CSRZ-DPSK)	12	11	6

The resolution bandwidth of the spectrum analyzer is set as 0.001 nm. It is observed that in the no-approximation model, the converted signal power spectrum of CSRZ-DPSK is narrower than other DPSK data formats.

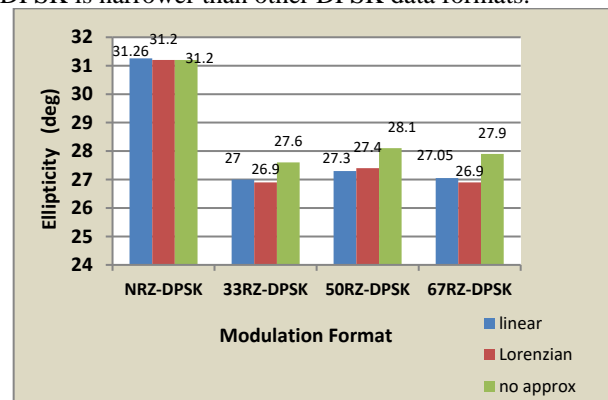


Figure 4. Ellipticity angle for different data formats and material gain simulation models

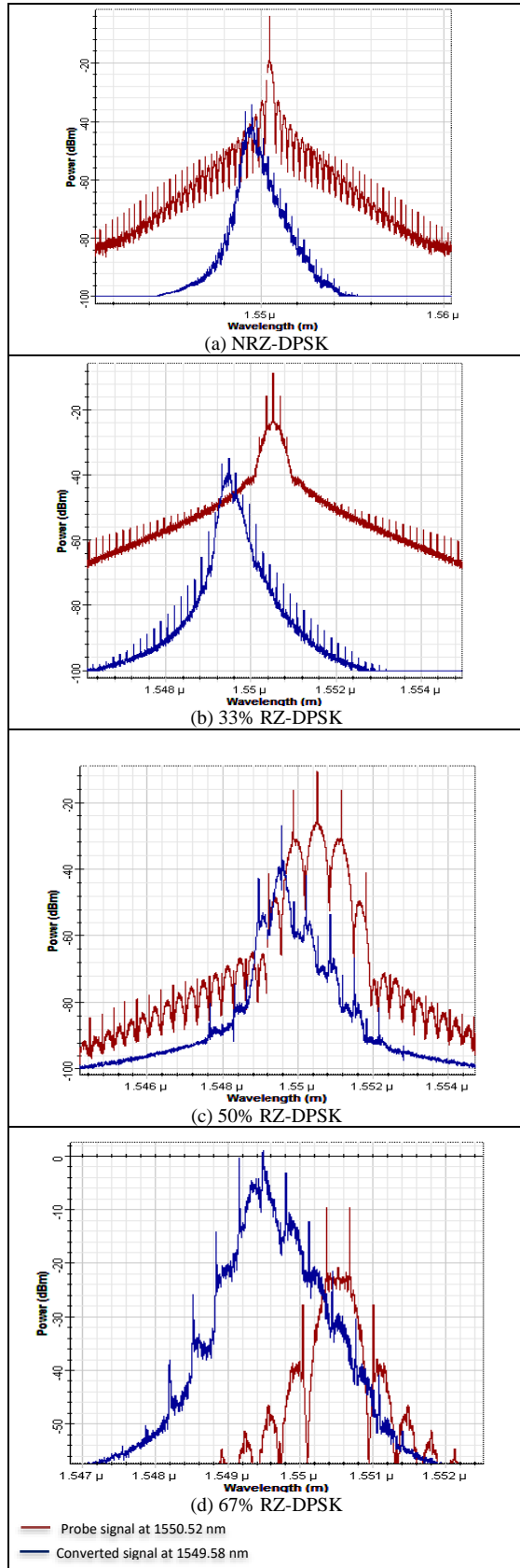


Figure 5. Different DPSK modulation dual spectra for the linear material gain ( $g_m$ ) simulation model

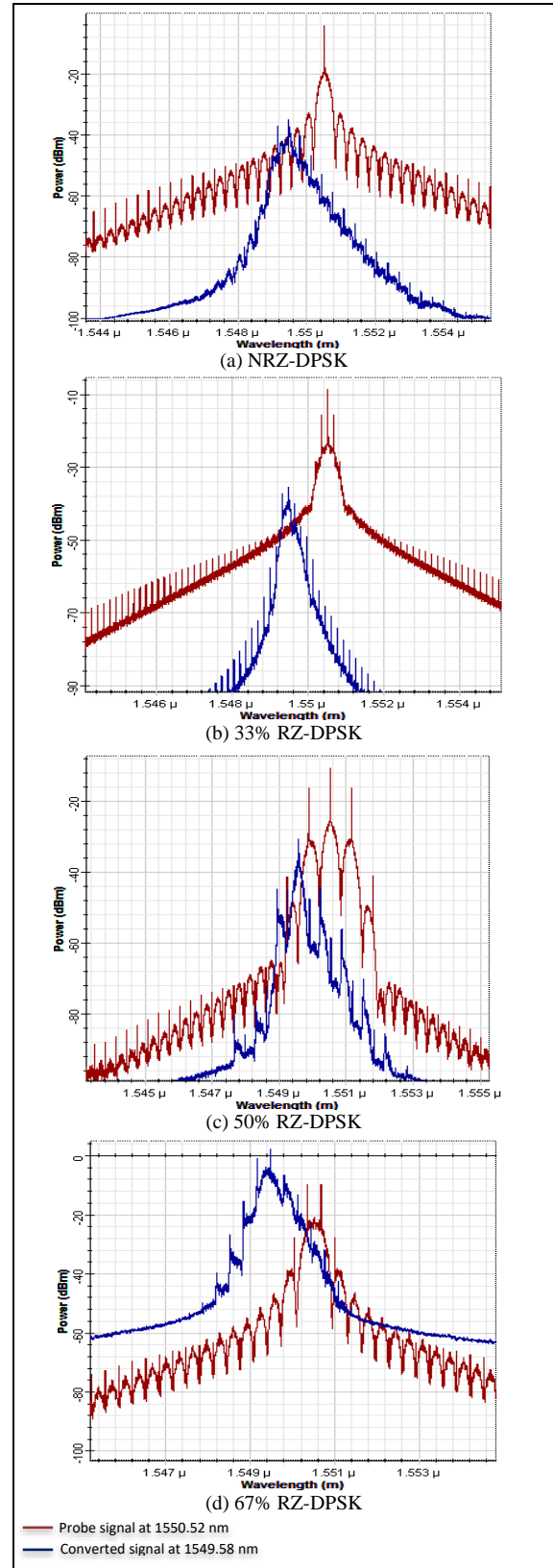


Figure 6. Different DPSK modulation dual spectrum for the Lorentzian material gain ( $g_m$ ) simulation model



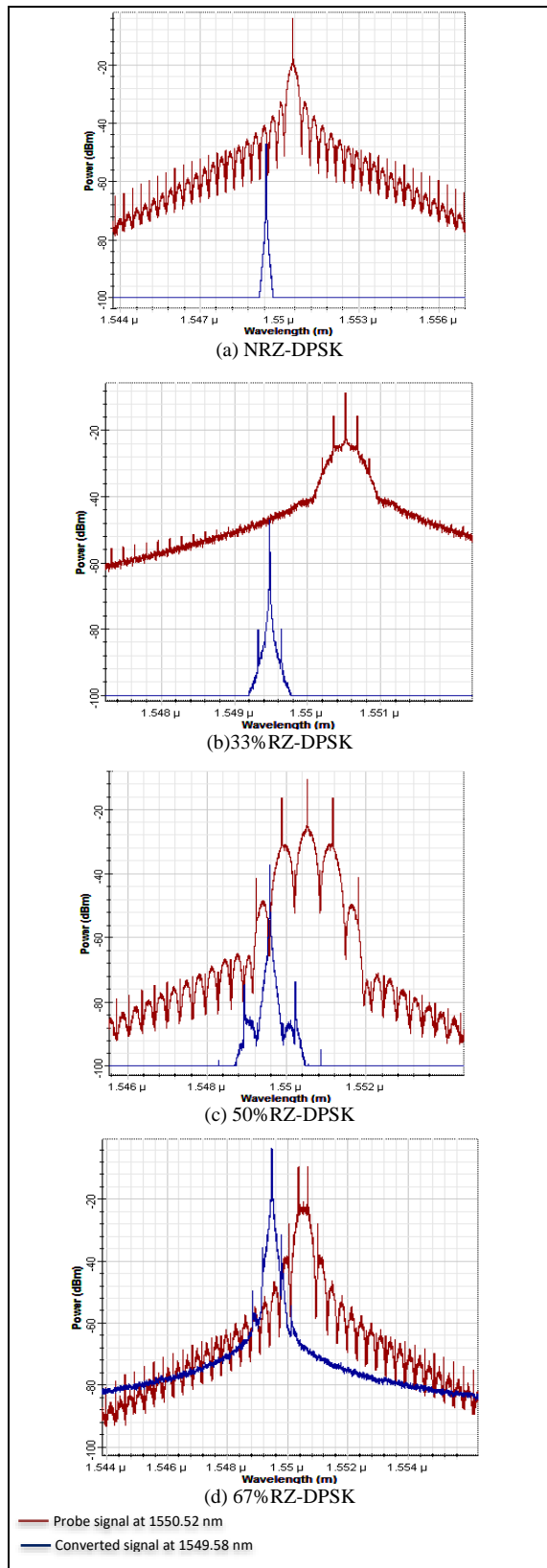


Figure 7. Different DPSK modulation dual spectrum for the no-approximation material gain ( $g_m$ ) simulation model

For all NRZ-DPSK, 33% RZ-DPSK, and 50% RZ-DPSK a negative output power spectral gain is obtained. But CSRZ-DPSK exhibits positive power spectral gain of 12 dB, 11 dB and 6 dB for Linear, Lorentzian and No-approximation simulation models respectively. The most attractive feature of CSRZ-DPSK is that it has a power spectral gain of up to 12 dB at a converted signal wavelength of 1549.48 nm. Table 4 shows the output spectral power gain for all DPSK formats.

## V CONCLUSION

In this research the effectiveness of various optical differential phase modulations on wavelength conversion is investigated. The NRZ-DPSK, 33% RZ-DPSK, 50% RZ-DPSK and CSRZ are analyzed. Using the non-linear polarization (NPR) phenomena inside the wide band SOA, XPolM-based AOWC is achieved by a suitable configuration. The data rate is 80 Gb/s. The experiment is continued for different material gain ( $g_m$ ) simulation models. The comparisons are made in terms of the amount of power coupled (dBm), ellipticity angles (degree) and optical power spectral gain (dB). The pump signal is set at a wavelength of 1549.48 nm with a power of -4 dBm. The input probe signal power is 1 dBm. With the 0.001 resolution bandwidth, the input and the converted signal spectra are analyzed. The NRZ-DPSK performs better in terms of maximum intensity coupled with the converted signal and ellipticity angle. However, the 67% RZ-DPSK/CSRZ-DPSK has shown to be a potential option in terms of power spectral gain. Linear, Lorentzian and no-approximation models of CSRZ-DPSK produce a spectral gain of 12 dB, 11 dB and 6 dB, respectively. The channel capacity of the WDM system can be enhanced since the main lobe of the CSRZ-DPSK with no-approximation of the material gain model is narrower than others. Altogether the CSRZ-DPSK with No-approximation of the material gain simulation model is shown to be a good choice.

## REFERENCES

- [1] S. J. B. Yoo, "Optical Packet and Burst Switching Technologies for the Future Photonic Internet", in *Journal of Lightwave Technology*, vol. 24, no. 12, pp. 4468-4492, 2006, <https://doi.org/10.1109/JLT.2006.886060>.
- [2] Abd El-naser A. Mohamed, et., "All Optical Bidirectional Wavelength Conversion Using Single Wide Band Traveling Wave Semiconductor Optical Amplifier", *Menoufia J. of Electronic Engineering Research (MJEER)*, Vol. 29, No. 1, 2020, <https://dx.doi.org/10.21608/mjeer.2020.69182>
- [3] Aneesh Sobhanan, Aravind Anthur, et., "Semiconductor optical amplifiers: recent advances and applications", *Adv. Opt. Photon.* 14, 571-651 (2022). <https://doi.org/10.1364/AOP.451872>
- [4] A.D. Ellis, A.E. Kelly, D. Nesses, "Error free 100 Gbit/s wavelength conversion using grating assisted cross-gain modulation in 2mm long semiconductor amplifier", *IET Electronics Letters*. 34(20), pp. 1958-1959, 1998, <https://doi.org/10.1049/el:19981214>
- [5] A. Matsumoto, K. Nishimura, K., "Operational design on high-speed semiconductor optical amplifier with assist light for application to wavelength converters using cross-phase modulation", *IEEE Journal of Quantum Electronics*, vol. 42, no. 3, pp. 313-323, 2006, <https://doi.org/10.1109/JQE.2006.869809>
- [6] S. H. Lee and J. I. Song, "An XPolM-Based All-Optical SSB Frequency Up-Conversion Technique in an SOA," in *IEEE*

- Photonics Technology Letters, vol. 29, no. 7, pp. 627-630, 2017, <https://doi.org/10.1109/LPT.2017.2676122>
- [7] Sunish Kumar Orappanpara Soman, "A tutorial on fiber Kerr nonlinearity effect and its compensation in optical communication systems", *Journal of Optics*, Volume 23, Number 12, 2021. <https://doi.org/10.1088/2040-8986/ac362a0>
- [8] Tang H, Yang C, Qin L, Liang L, et., "A Review of High-Power Semiconductor Optical Amplifiers in the 1550 nm Band. Sensors (Basel)", 2023 Aug 22;23 (17):7326. <https://doi.org/10.3390/s23177326>
- [9] R. Shuai, X. Guijin, X. Yinghui, Z. et., "Research on Performance of Optical DPSK Modulation Format in All Optical Network", 10th International Conference on Communication Software and Networks (ICCSN), Chengdu, China, 2018, pp. 65-68, 2018, <https://doi.org/10.1109/ICCSN.2018.8488317>
- [10] Zhihong Li, Yi Dong, Jinyu Mo, et., "1050-km WDM transmission of 8/spl times/10.709Gb/s DPSK signal using cascaded in-line semiconductor optical amplifier", in IEEE Photonics Technology Letters, vol. 16, no. 7, pp. 1760-1762, July 2004, <https://doi.org/10.1109/LPT.2004.828521>
- [11] S. R. Chinn, D. M. Boroson and J. C. Livas, "Sensitivity of optically preamplified DPSK receivers with Fabry-Perot filters", in *Journal of Lightwave Technology*, vol. 14, no. 3, pp. 370-376, 1996, <https://doi.org/10.1109/50.485595>
- [12] W. A. Atia and R. S. Bondurant, "Demonstration of return-to-zero signaling in both OOK and DPSK formats to improve receiver sensitivity in an optically preamplified receiver", 1999 IEEE LEOS Annual Meeting Conference Proceedings. LEOS'99, 12th Annual Meeting. IEEE LEOS Annual Meeting (Cat. No.99CH37009), San Francisco, CA, USA, pp. 226-227 vol.1, 1999, <https://doi.org/10.1109/LEOS.1999.813561>
- [13] Mauro, J.C., Raghavan, S, "Advanced modulation formats for fiber optic communication systems", *Scientific Modeling and Simulation*, 15, 283-312, 2008, <https://doi.org/10.1007/s10820-008-9106-0>
- [14] A. H. Gnauck and P. J. Winzer, "Optical phase-shift-keyed transmission, *Journal of Lightwave Technology*", vol. 23, no. 1, pp. 115-130, 2005, <https://doi.org/10.1109/JLT.2004.840357>
- [15] Brendan F Surre KF Philippe S et., "The use of polarization effects in semiconductor optical amplifiers to perform all-optical signal processing ingeniería", *Revista chilena de ingeniería*. 15(3):313-319, 2007, <http://dx.doi.org/10.4067/S0718-33052007000300011>
- [16] Sarojini, R., Sivanantharaja, A. & Selvendran, S, All-optical wavelength conversion of 80 gbps CSRZ-DPSK data signal using cross polarization modulation in single wideband SOA with sub-mw pump power", *Opt Quant Electron* 54, 314, 2022. <http://dx.doi.org/10.1007/s11082-022-03540-y>
- [17] Agrawal GP "Fiber-Optic Communication Systems", 4th edition. Wiley. Germany, 2012.
- [18] Ahvan Sharifi, Mohammad Razaghi and Vahid Ahmadi, "Analysis of nonlinear polarization rotation by an ultrashort optical pump and probe pulse in a strained semiconductor optical amplifier", *Journal of the Optical Society of America B*, , 36(2), pp.374-382, 2019, <https://doi.org/10.1364/JOSAB.36.000374>
- [19] Xianghua Feng, Jiarong Ji Guomin Zhang, "Nonlinear Polarization Rotation Characteristic Phenomenon in a Bulk Semiconductor Optical Amplifier", *Optics and Photonics Journal*, 3(2B):187-191, 2013, <https://doi.org/10.4236/opj.2013.32B045>
- [20] B.F. Kennedy, S. Philippe, et., "Experimental investigation of polarisation rotation in semiconductor optical amplifiers", *Optoelectronics*, 2004, IEE Proceedings. 151(2):114 - 118, <https://doi.org/10.1049/ip-opt:20040287>
- [21] M J Connelly, "Wideband semiconductor optical amplifier steady-state numerical model", *IEEE Journal of Quantum Electronics*, 37(3): 439-447, 2001, <https://doi.org/10.1109/3.910455>
- [22] M. Menif, P. Lemieux, W. et., "Incoherent-to-coherent wavelength conversion using semiconductor optical amplifier", *IEEE International Conference on Communications (IEEE Cat. No.04CH37577)*, Paris, France, pp. 1740-1744 Vol.3, 2004, <https://doi.org/10.1109/ICC.2004.1312806>